PASJ: Publ. Astron. Soc. Japan **52**, 499–508 (2000)

Slim-Disk Model for Soft X-Ray Excess and Variability of Narrow-Line Seyfert 1 Galaxies

Shin MINESHIGE and Toshihiro KAWAGUCHI
Department of Astronomy, Graduate School of Science, Kyoto University, Sakyo-ku, Kyoto 606-8502
E-mail (SM): minesige@kusastro.kyoto-u.ac.jp

Mitsuru TAKEUCHI
Astronomical Institute, Osaka-Kyoiku University, Asahigaoka, Kashiwara 582-8582
and
Kiyoshi HAYASHIDA
Department of Earth and Space Sciences, Graduate School of Science, Osaka University, Toyonaka 560-0043

(Received 1999 December 22; accepted 2000 February 17)

Abstract

Narrow-line Seyfert 1 galaxies (NLS1s) exhibit an extreme soft X-ray excess and large variability. We argue that both features can be basically accounted for by the slim-disk model. We assume that a central black-hole mass in NLS1 is relatively small, $M \sim 10^{5-7} M_\odot$, and that a disk shines nearly at the Eddington luminosity, $L_{\rm E}$. Then, the disk becomes a slim disk and exhibits the following distinctive signatures: (1) The disk luminosity (particularly of X-rays) is insensitive to the mass-flow rates, $\dot{M}$, since the generated energy is partly carried away to the black hole by trapped photons in accretion flow. (2) The spectra are multi-color blackbody. The maximum blackbody temperature is $T_{\rm bb} \simeq 0.2 (M/10^5 M_\odot)^{-1/4}$ keV, and the size of the blackbody emitting region is small, $r_{\rm bb} \lesssim 3 r_{\rm S}$ (with $r_{\rm S}$ being Schwarzschild radius), even for a Schwarzschild black hole. (3) All of the ASCA observation data of NLS1s fall onto the region of $\dot{M}/(L_{\rm E}/c^2) > 10$ (with $L_{\rm E}$ being the Eddington luminosity) on the $(r_{\rm bb}, T_{\rm bb})$ plane, supporting our view that a slim disk emits soft X-rays at $\sim L_{\rm E}$ in NLS1s. (4) Magnetic energy can be amplified, at most, up to the equipartition value with the trapped radiation energy, which greatly exceeds the radiation energy emitted from the disk. Hence, energy release by consecutive magnetic reconnection will give rise to substantial variability in soft X-ray emission.

Key words: accretion, accretion disks — black holes — galaxies: active — galaxies: Seyfert

1. Introduction

The terminology of *narrow-line* Seyfert 1 galaxies (NLS1s) originates from their relatively *narrow* optical Balmer-line emission with $v_{\rm BLR} \lesssim 2000$ km s^{-1} compared with those of usual Seyfert 1 galaxies with broad-line emission, BLS1s (see a concise review by Brandt 1999 and references therein). Their optical line ratios and remarkable Fe II lines (Osterbrock, Pogge 1985; Halpern, Oke 1987; Grupe et al. 1999) are also distinct from those of BLS1s. NLS1s exhibit unique X-ray properties (e.g., Grupe et al. 1998); they are characterized by large soft X-ray excess (Pounds et al. 1996; Otani et al. 1996; Leighly 1999b) and a good correlation is known to exist between the strength of the soft excess and FWHM of optical Balmer lines (Boller et al. 1996; Laor et al. 1997). Rapid soft/hard X-ray variability is another signature characterizing NLS1s (Otani et al. 1996; Boller et al. 1997; Leighly 1999a). NLS1s are not rare, but comprise a significant part (say, 20%) of the Seyfert 1 galaxies, and it seems that a group of NLS1s is smoothly connected to the class of BLS1s (Brandt, Boller 1998).

It is often suggested that the strength of the soft X-ray excess relative to the hard X-ray power law appears to be directly related to the 'primary eigenvector' of Boroson and Green (1992), which represents the strongest set of optical emission-line correlations (e.g., Brandt 1999). In this sense, NLS1s are located at the extreme end of the primary eigenvector. The UV line properties of NLS1s also fit this scheme (Wills et al. 1999). Then, what is the control parameter which drives the primary eigenvector? What physical factor distinguishes NLS1s from BLS1s?

There are several models proposed to account for the narrowness of otherwise broad-line emission (see Boller et al. 1996 for extensive discussion). Successful models should account for a smooth continuation between NLS1s and BLS1s. Among them, one fascinating and probably most-promising explanation is that NLS1s contain relatively less massive black holes (with $M \sim 10^{5-7} M_\odot$).

The moderate brightness of NLS1s, $L \sim 10^{43-45}$ erg s^{-1}, implies similar mass-flow rates, $\dot{M}$, to those of BLS1s. It then follows that the ratio $L/L_{\rm E}$ (or $\dot{M}/M$) is relatively large for NLS1s. The control parameter which drives the eigen vector could be the fraction of the Eddington rate at which the supermassive black hole is accreting, $\dot{M}/(L_{\rm E}/c^2)$.

For small black-hole masses, narrow Balmer-line emission of NLS1s can be understood, provided that the broad-line clouds (which emit broad-line emission in BLS1s) are bound in the potential by a central black hole (Laor et al. 1997). Since the radius of the broad-line clouds is roughly scaled as $r_{\rm BLR} \propto L^{0.5}$ from the reverberation mapping (Kaspi et al. 1996), the circular velocity of broad-line clouds, $\sim \sqrt{GM/r_{\rm BLR}}$, is systematically smaller for smaller M at a constant L (and thus constant $r_{\rm BLR}$), yielding narrow Balmer emission.

When closing to the Eddington luminosity,

$$L_{\rm E} \simeq 1.2 \times 10^{43} M_5 \ {\rm erg\ s^{-1}}, \tag{1}$$

where $M_5 \equiv M/(10^5 M_\odot)$, what do we then expect theoretically for the disk structure and its spectra? It is known that for such a high-luminosity advective energy transport dominates over radiative cooling (Abramowicz et al. 1988; section 10.3 of Kato et al. 1998). Such a disk is named "slim disk", since it is moderately geometrically thick.

The slim disk is an optically thick version of ADAF (advection-dominated accretion flow) and should not be confused with optically thin ADAF proposed for low-luminosity AGNs (see section 10.2 of Kato et al. 1998 and references therein). Unlike the optically thin ADAF, the observable features of the slim disk have been poorly investigated. Szuszkiewicz et al. (1996) was the first to start an investigation along this line (see also Wang et al. 1999); we give a more detailed discussion on the observational consequences in the present study. Watarai et al. (2000) studied the super-critical accretion flow in the context of galactic black-hole candidates (GBHC), showing some unique observational features of the slim disk.

We focus on the AGN case in the present study. The calculation methods are given in section 2. We then discuss the non-standard emission properties of the slim disk in the context of NLS1s in section 3. We next turn to the subject of large variability and discuss its origin in relation to magnetic-field activity in section 4. Outstanding issues are discussed in section 5. The final section is devoted to conclusions. Throughout the present study we use the normalization of $\dot{M}$ with $\dot{M}_{\rm crit} \equiv L_{\rm E}/c^2$; i.e.,

$$\dot{m} \equiv \dot{M}/\dot{M}_{\rm crit} \sim \dot{M}/(1.3 \times 10^{22} M_5 \ {\rm g\ s^{-1}}) \sim \dot{M}/(2.5 \times 10^{-4} M_5 \ M_\odot \ {\rm yr^{-1}}). \tag{2}$$

2. Basic Equations and Calculation Methods

We first solve the steady-state, transonic disk structure. Although the methods used are the same as those adopted in Matsumoto et al. (1984) and Watarai et al. (2000), we briefly repeat the description below.

For the purpose of the present study, it is essential to solve the full-set equations, since the emission from the innermost region is in question. (Approximate solutions, such as self-similar solutions, do not properly treat the inner boundary conditions nor regularity conditions.) The transonic nature of the accretion flow should also be carefully treated. We do not include any general relativistic (GR) effects, except for adopting the pseudo-Newtonian potential by Paczyński and Wiita (1980), $\psi = -GM/(r - r_{\rm S})$. For a discussion of GR effects, see subsection 3.5. We use cylindrical coordinates (r, φ, z).

Throughout the present study, we used vertically integrated (or height-averaged) equations. In fact, we numerically confirmed that $H/r < 1$ for $\dot{m} \lesssim 100$, where H is the scale-height of the disk. Certainly, $H/r > 1$ for even a higher mass accretion rate, but for such high $\dot{m}$, the photon-diffusion time over H becomes longer than the accretion timescale, so that the disk height should be significantly reduced (see subsection 5.1). The height-average approach may not be very precise, and we eventually need fully 2-D models. The same problem arises in optically thin ADAF, for which Narayan and Yi (1995) found that the 2-D solutions of the exact non-height-integrated equations agree quite well with those of the simplified height-integrated equations, provided that 'height-integration' is done along θ at constant spherical radius, rather than along z at constant cylindrical radius. The height-integrated equations are therefore a fairly accurate representation of quasi-spherical ADAFs.

We construct the vertically integrated equations, using integrated variables, such as surface density, $\Sigma \equiv \int \rho dz$, and integrated pressure, $\Pi \equiv \int p dz$. Vertically integrated mass, momentum, and angular-momentum conservations lead to

$$-2\pi r \Sigma v_r = \dot{M} = {\rm const.}, \tag{3}$$

$$v_r \frac{dv_r}{dr} + \frac{1}{\Sigma}\frac{d\Pi}{dr} = \frac{\ell^2 - \ell_{\rm K}^2}{r^3} - \frac{\Pi}{\Sigma}\frac{d\ln \Omega_{\rm K}}{dr}, \tag{4}$$

and

$$\dot{M}(\ell - \ell_{\rm in}) = -2\pi r^2 T_{r\varphi}, \tag{5}$$

respectively, where Ω $(= v_\varphi/r)$ and $\Omega_{\rm K}$ $[= (GM/r)^{1/2}/(r - r_{\rm S})]$ are the angular frequency of the gas flow and the Keplerian angular frequency in the pseudo-Newtonian potential, ℓ $(= r v_\varphi)$ is the specific angular momentum, $\ell_{\rm K}$ $(\equiv r^2 \Omega_{\rm K})$ is the Keplerian angular momentum, $\ell_{\rm in}$ is the specific angular momentum finally swallowed by the black hole, and $r_{\rm S} \equiv 2GM/c^2 \simeq 3 \times 10^{10} M_5$ cm is the

Schwarzschild radius. As for the viscous stress tensor, we adopt the prescription $T_{r\varphi} \equiv -\alpha\Pi$ with the viscosity parameter, $\alpha = 0.1$. Note, however, that the resultant disk structure does not sensitively depend on α (K. Watarai et al. 2000 in preparation).

The vertically integrated energy equation is symbolically written as

$$Q^-_{\rm adv} = Q^+_{\rm vis} - Q^-_{\rm rad}, \qquad (6)$$

where $Q^-_{\rm adv}[\propto \Sigma v_r T(ds/dr)]$ is the advective cooling with s being the specific entropy; the other two terms on the right-hand side represent viscous heating and radiative cooling, respectively.

The outer-boundary conditions are imposed at $r = 2.0\times10^3\, r_{\rm S}$, where each physical quantity is taken as that of the standard disk. We confirmed that the disk structure near the outer boundary can be very accurately described by the standard-disk relation. When calculating the spectra (see below), we extrapolate the temperature distribution up to $r = 2.0\times10^4\, r_{\rm S}$ using the standard-disk relation, $T_{\rm eff} \propto r^{-3/4}$. The basic equations are integrated by the semi-implicit method from the outer boundary to the inner one taken at $r = 1.01\, r_{\rm S}$. The flow is subsonic far outside ($r \gg r_{\rm S}$), but is supersonic just near the black hole. The solution should satisfy the regularity condition at the transonic radius, at about 2.7 $r_{\rm S}$, and we adopt the free boundary conditions at the inner edge.

3. Observational Features of a Slim Disk

3.1. *Unique Temperature Profile*

How do structural changes occur from the standard to the slim disk when $\dot{m}$ increases? The solid lines in the upper panels of figure 1 represent the temperature profiles of the disks for various values of $\dot{m}$ for a black-hole mass of $M = 10^5 M_\odot$. For a comparison, we also plot with dashed lines the temperatures expected from the standard-disk relation (Shakura, Sunyaev 1973),

$$T_{\rm eff} \simeq 10^{6.5} M_5^{-\frac{1}{4}} \dot{m}^{\frac{1}{4}} \left(\frac{r}{r_{\rm S}}\right)^{-\frac{3}{4}} \left(1 - \sqrt{\frac{r_{\rm in}}{r}}\right)^{\frac{1}{4}} {\rm K}, \qquad (7)$$

where $M_5 \equiv M/10^5 M_\odot$.

We note three characteristics:

1. In contrast with the standard disk having an effective temperature profile of $T_{\rm eff} \propto r^{-3/4}$, the slim disk exhibits flatter slopes, $T_{\rm eff} \propto r^{-1/2}$ (Watarai, Fukue 1999). As $\dot{m}$ increases, the part with a flatter temperature profile expands outward: i.e., up to $r \sim 100\, r_{\rm S}$ for $\dot{m} \sim 100$, and $r \sim 1000\, r_{\rm S}$ for $\dot{m} \sim 1000$.

2. When the innermost parts become advection-dominated at $\dot{m} \gtrsim 50$, a substantial amount of radiation is expected from inside the marginally stable last stable orbit, $r_{\rm ms} = 3\, r_{\rm S} \sim 10^{11}$ cm. This can be understood as follows. For $\dot{m} \ll 1$, the flow is very subsonic far outside, while it should become supersonic near the black hole. A sudden jump in the radial accretion velocity across the transonic radius (at $\sim 2.7\, r_{\rm S}$) results in an abrupt density drop inside the transonic radius (note $\dot{M} \propto v_r\Sigma$ is kept constant). The innermost region becomes of low density, thus producing little emission (emissivity goes like ρ^2). For $\dot{m} \gtrsim 50$, conversely, the flow velocity outside the transonic radius is already comparable to the sound speed; thus, the velocity and density jump across the transonic radius being small. Therefore, a huge, continuous mass supply makes it possible to keep the innermost region (at $r < 3\, r_{\rm S}$) optically thick and a substantial amount of radiation can be produced there as a result.

3. Consequently, the inner-disk temperature (which makes a hotter peak in the spectrum) becomes sys-

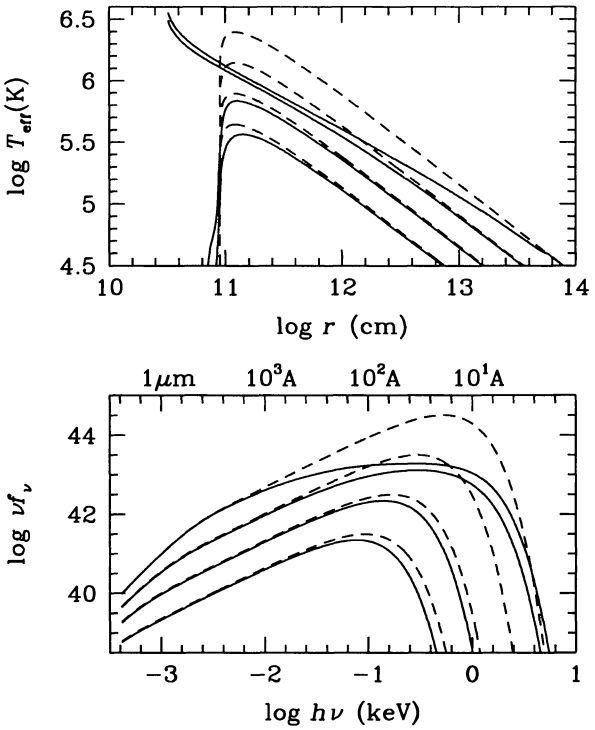

Fig. 1. Temperature profiles (upper) and the emergent spectra (lower) of the calculated disks with different mass-flow rates: $\dot{m} = 1.0$, 10.0, 100.0, and 1000.0 from below by the solid lines. As $\dot{m}$ increases, regions with a flat temperature profile (extending down to $\log r \sim 10.5$ or $r \sim r_{\rm S}$) expand from the innermost region and the disk spectra become flatter at the peak. For a comparison, we plot the temperature profiles expected by the standard-disk relation [equation (7)] and their emergent spectra by the dashed lines.

tematically higher than the values expected by the standard relation. The size of the region emitting with the maximum energy becomes small, however.

3.2. *Spectral Features*

Once temperature distributions are obtained, we can calculate the emergent spectra by simply summing up the contribution from each tiny portion of the disk. Such scattering-dominated hot disks, like those considered here, do not always emit blackbody radiation (Czerny, Elvis 1987; Beloborodov 1998). However, we simply assume blackbody radiation to see the effects of transonic flow (discussed later).

The results are plotted in the lower panels of figure 1. As $\dot{m}$ increases, the spectra, νS_ν, become flatter and flatter around the peak, $\nu S_\nu \sim \nu^0$. (Still, $\nu S_\nu \sim \nu^{4/3}$ in the optical bands.) According to Grupe et al. (1998) soft X-ray selected AGNs (including a number of NLS1s) tend to exhibit a bluer optical/UV (around 1400 Å) spectra when compared with those of hard X-ray selected ones, and the maximum slope is $S_\nu \propto \nu^{0.3}$. This is consistent with our calculations.

The most significant problem lies in $a_{\rm os}$, or the optical-to-soft X-ray flux ratio (say 3000 Å to 0.2 keV). High $L/L_{\rm E}$ models predict a very flat $a_{\rm os}$, -1 or flatter, as shown in figure 1, whereas the observed slope is more like -1.5 (see table 1 of Brandt et al. 2000, which includes many NLS1s; however, see Edelson et al. 1999). Thus, the observed soft X-ray emission is a factor of 10, or more, weaker than that in high $L/L_{\rm E}$ disk models. In fact, this problem already exists for normal AGNs (Laor et al. 1997) and is actually more severe for NLS1s because of the flatter predicted $a_{\rm os}$. This does not necessarily rule out the disk model, but may suggest a significantly reduced efficiency of the emission from the inner parts of the accretion disk (e.g., Laor 1998).

NLS1s have a steeper soft (0.1–2 keV) X-ray slope, but since they have a fairly normal $a_{\rm os}$, this slope is actually mostly because the hard X-ray component is weak, and not because the soft component is strong (Laor et al. 1997). The slim-disk model shows that exponential roll-over extends over 1 keV, thus producing large power-law indices in the ROSAT band. The inclusion of Compton scattering within the disk will increase the photon indices further (Ross et al. 1992), which is discussed in subsection 3.5. A fairly strong correlation between the optical and soft X-ray emission is naturally explained, since both are from the same optically thick disk.

If we include a hard power-law component in the calculation, we expect a larger hard power-law index in the ASCA bands for a larger soft excess as the result of more efficient cooling of electrons via inverse Compton scattering. Since the hard power-law slope is determined by the Compton y-parameter, which is related to the energy amplifications of soft photons (e.g. Rybicki, Lightman 1979), less (or more) energy input to high-energy electrons compared with that to soft photons leads to a smaller (larger) y and thus a larger (smaller) photon index in the hard X-ray bands; $\alpha_{\rm x} \gtrsim 2$ ($\alpha_{\rm x} < 2$) as is observed in the soft (hard) state of GBHC (Mineshige et al. 1995). Systematically large $\alpha_{\rm x}$'s in NLS1s in the ASCA bands (Pounds et al. 1996; Brandt et al. 1997) can be understood.

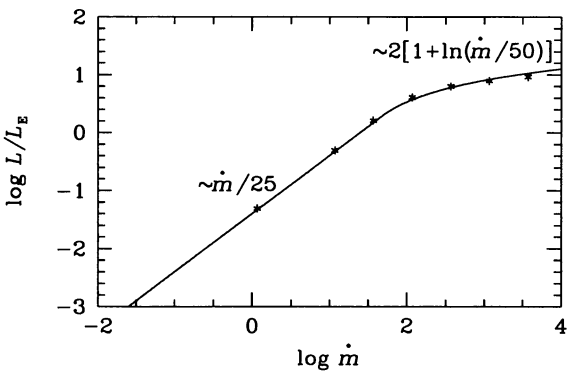

Fig. 2. Disk luminosity as a function of $\dot{m}$. The asterisks denote the calculated luminosities, whereas the solid line shows the fitting formula (8). It is clear that an increase in L is suppressed at $L > 2L_{\rm E}$.

Further, Tanaka (1989) found highly variable hard emission relative to the soft one in GBHC. If the analogy holds, the relative strength of the hard component could take any values. This may explain a diversity in $\alpha_{\rm x}$'s of NLS1s in the ASCA bands.

3.3. *Evolution of the Disk Luminosity*

It should be repeated that the disk luminosity increases only moderately above $L_{\rm E}$ for steadily increasing $\dot{M}$. We calculated L by summing up the contribution from each concentric annulus and plot it in figure 2 as a function of $\dot{m}$. The asterisks are the calculated values, while the solid curve represents the fitting formula (see Watarai et al. 2000 for a derivation),

$$L(\dot{m})/L_{\rm E} \simeq \begin{cases} 2\,[1+\ln(\dot{m}/50)] & \text{for } \dot{m} \geq 50 \\ \dot{m}/25 & \text{for } \dot{m} < 50. \end{cases} \quad (8)$$

The functional dependence of $L/L_{\rm E}$ on $\dot{m}$ is basically the same as that for GBHC with smaller black-hole masses, thus being insensitive to M.

Care must be taken when interpreting L, since the radiation field is likely to be anisotropic; i.e., radiation mostly goes out in the vertical direction to the disk plane, whereas matter approaches to the black hole along the disk plane. This is a way in which super-critical accretion is possible; but at the same time, we expect much diluted radiation going out in the direction of the disk plane. Blocking of the radiation by the outer disk rim provides

Table 1. Results of fitting.

$\dot{m}$	$\log T$(K)	$T_{\rm in}$(keV)	$\log r_{\rm in}$(cm)	$r_{\rm in}/r_{\rm S}$	p
10^{0}	5.57	0.033	11.45	9.34	0.88
$10^{0.5}$	5.71	0.044	11.39	8.20	0.78
$10^{1.0}$	5.84	0.061	11.34	7.19	0.74
$10^{1.5}$	6.06	0.098	11.05	3.74	0.62
$10^{2.0}$	6.46	0.252	10.24	0.58	0.52
$10^{2.5}$	6.53	0.294	10.12	0.44	0.50
$10^{3.0}$	6.55	0.303	10.14	0.46	0.51
$10^{3.5}$	6.56	0.310	10.13	0.45	0.51

an additional diluting effect (Fukue 2000). Thus, we will detect weaker flux [$< L_{\rm E}/(4\pi d^2)$ with d being distance], even when the total L exceeds $L_{\rm E}$. We also expect a strong radiation-accelerated wind in the central region (e.g., Watarai, Fukue 1999), which will give rise to blue-shifted UV lines (Leighly 1999b).

3.4. *Fitting with the Multi-Color Blackbody*

We now fit the calculated disk spectra by the extended disk blackbody model (Mineshige et al. 1994a), assuming the following $T_{\rm eff}$ profile:

$$T_{\rm eff} = T_{\rm in}(r/r_{\rm in})^{-p}, \tag{9}$$

where $r_{\rm in}$, $T_{\rm in}$, and p are fitting parameters.

Note that the fitting results may slightly depend on the X-ray energy ranges for which fitting is made, but in the present study we fix the energy bands to be either 0.1–0.5 keV (for $\dot{m} < 10$), 0.1–1.0 keV (for $10 \leq \dot{m} < 100$), or 0.1–3.0 keV (for $\dot{m} \geq 100$).

To have a good fitting result, especially in p, wider spectral ranges, especially a good coverage of the soft X-ray bands, are certainly necessary. The small black-hole mass is preferable for this sort of fitting, since in this case the disk temperature is roughly scaled as $\sim M^{-1/4}$, as expected from the standard-disk relation (which is also roughly valid in the slim-disk regime). In the fitting, $T_{\rm in}$ and $r_{\rm in}$ are basically determined by the energy and the intensity of the exponential roll-over, while p depends on the slope in the lower energy bands. EUV to soft X-ray observations are crucial for discriminating the slim disk from the standard disk.

We examine how the derived fitting parameters of $r_{\rm in}$, $T_{\rm in}$, and p change with an increase of the mass-flow rate (and L). The results of the fittings are summarized in table 1 and figure 3.

As $\dot{m}$ increases, so does $T_{\rm in}$, more or less gradually; but at the same time $r_{\rm in}$ shifts from $\sim 10\ r_{\rm S}$ to $\sim 0.5\ r_{\rm S}$ abruptly at $L/L_{\rm E} \sim 2$ ($\dot{m} \sim 50$). We should recall that $r_{\rm in}$ stands for the size of the area emitting with $B_\nu(T_{\rm in})$, and not the radius of the physical inner boundary (which should be always at $r_{\rm S}$). In fact, the upper part of figure 1 has already shown that the peak effective temperature shifts toward smaller radii as $\dot{m}$ increases.

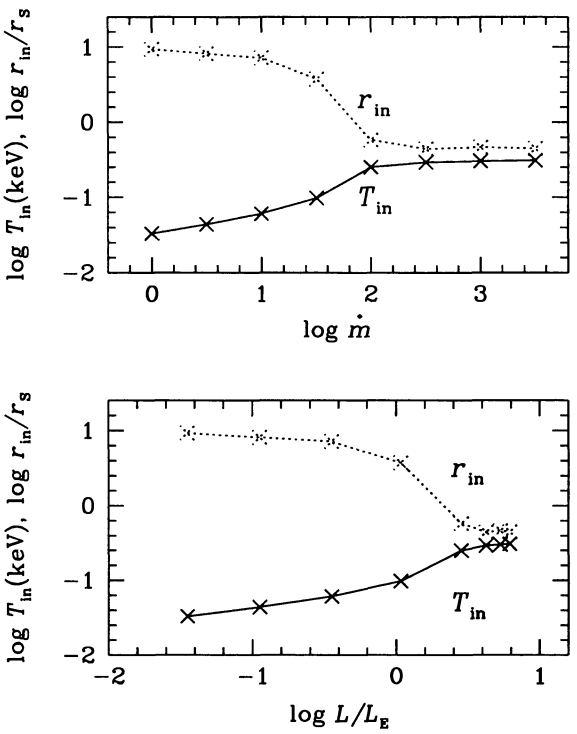

Fig. 3. Results of the fitting, $r_{\rm in}$ (by the dotted lines) and $T_{\rm in}$ (by the solid lines), as functions of $\dot{m}$ (upper) and of $L/L_{\rm E}$, respectively.

The effective temperature of the slim disk has a weak luminosity dependence, $T_{\rm in} \propto M^{-1/4} \propto L^{-1/4}$; however, $T_{\rm in}$ also has some dependence on $\dot{M}/M$ at $\dot{m} < 50$. We, hence, expect scatters in $T_{\rm in}$, even for the same M and L.

3.5. *Comparison with the Observations*

Hayashida (2000) analyzed the ASCA spectral data of 9 NLS1s and fitted them with a two spectral-component model: a hard power-law component and a soft blackbody one. We assume that the soft component represents the emission from the disk we are discussing. The fitting parameters of the soft component are the blackbody temperature, $T_{\rm bb}$, and the size of the blackbody emitting region, $r_{\rm bb}$. The results of the fitting are summarized in figure 4 and in table 2.

Note that the redshifts are small, $z < 0.1$, for all sources. Among the nine sources in Hayashida (2000), we excluded Mrk 766 because of its complex spectral features and their variability (Leighly et al. 1996). Even for the other eight sources, it must be kept in mind that there may be some model dependence in the data points of $T_{\rm bb}$

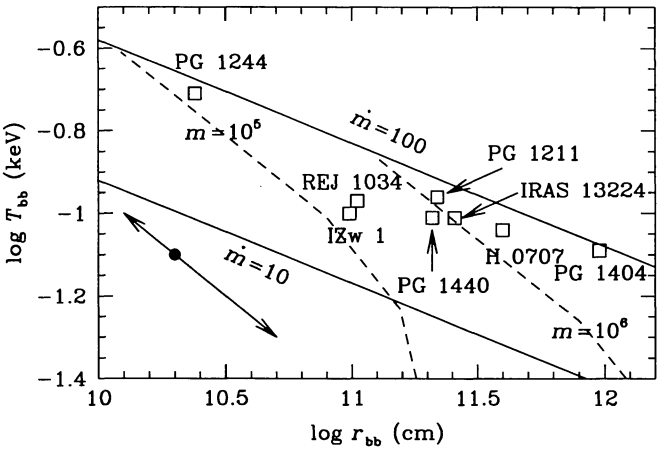

Fig. 4. r_{bb}–T_{bb} diagram of the observational data of NLS1s. The loci of $\dot{m} = 10$ and 100 (by the solid lines) and those of m ($\equiv M/M_\odot$) $= 10^5$ and $10^6 M_\odot$ (by the dotted lines) obtained by the slim disk are also shown ($i = 60°$ is assumed). The arrow aimed to the upper-left (or lower-right) from the filled circle in the lower-left corner indicates the direction of the correction for that point to remove Compton and GR effects in the case of a face-on (nearly edge-on) disk.

Table 2. Results of ASCA observations.

Source	T_{bb}(keV)	r_{bb}(cm)	$\log(T_{bb}^4 r_{bb})$
IZw 1	0.100	9.75×10^{10}	6.99
REJ 1034	0.107	1.04×10^{11}	7.14
PG 1440	0.097	2.08×10^{11}	7.28
IRAS 13224	0.098	2.55×10^{11}	7.38
H 0707	0.091	3.97×10^{11}	7.44
PG 1211	0.109	2.21×10^{11}	7.50
PG 1244	0.191	2.39×10^{10}	7.51
PG 1404	0.081	9.50×10^{11}	7.62

and in r_{bb}. In particular, modeling of peculiar spectral features around 1.1 keV found for some sources [IRAS 13224, H 0707, and PG 1404; see Hayashida (2000) and reference therein] affects the parameter T_{bb} significantly, e.g., T_{bb} for H 0707 might be about 30% higher than the value listed in table 2, if we model the feature as absorption edges. On the other hand, for sources of which the soft component are not so prominent, e.g., IZw 1, the results will be affected if we allow some deviation from the perfect power-law model for the hard component. The calibration problem of ASCA SIS may also add extra error to the results. These points will be addressed in a separate paper.

The theoretical expectations based on the slim disk model are also plotted by the solid and dashed lines in figure 4. Since the inclination angles are not known, we assume an inclination angle of $i = 60°$ in the theoretical models; i.e., we set $r_{bb} = r_{in}\sqrt{\cos i}$. Likewise, we set $T_{bb} = T_{in}$, although the former may be systematically higher than the latter, $T_{in} \simeq (1.1\text{–}1.3)T_{bb}$. Accordingly, the value of r_{bb} should be smaller, for $L \propto r_{bb}^2 T_{bb}^4$ is kept roughly constant. It might also be noted that the combination of $r_{bb}T_{bb}^4$, which is proportional to L/L_E, is mass-independent, since r_{bb} ($\propto r_{in}$) can be scaled with $r_S \propto M$ and $T_{bb} \sim T_{in} \propto M^{-1/4}$. Therefore, constant $\dot{m}$ lines give a relation, $T_{bb} \propto r_{bb}^{-1/4}$.

On theoretical grounds, various kinds of GR effects and Compton scattering should affect the results. When scattering opacity dominates over absorption, the emergent spectra deviate from the blackbody one (see Rybicki, Lightman 1979). In a hot disk with Compton $y > 1$, moreover, inverse Compton scattering should modify the disk spectra in the high-energy tail, thereby yielding, at most, a factor of 2 *increase* in T_{bb}, while the total flux ($\propto r_{bb}^2 T_{bb}^4$) is kept constant; i.e., a factor of 4 *decrease* in r_{bb} (Ross et al. 1992; Shimura, Takahara 1995).

GR effects (such as gravitational redshift, Doppler boosting, gravitational focusing due to ray bending) produce complex effects. We calculate a slim-disk model with face-on geometry, for which only a gravitational redshift works, finding a systematically *larger* r_{bb} ($\sim 3\ r_S$) by a factor of ~ 6 and thus *lower* T_{bb} (~ 0.12 keV) by a factor of ~ 2.5 even for $\dot{m} \gtrsim 100$. In other words, most of the radiation from inside $3\ r_S$ vanishes for this case. [Although photon energy gets lost partly, the total flux does not drop much because of flatter T_{eff} profile, $T_{eff}(r) \propto r^{-1/2}$.] Since Compton and GR effects work independently in opposite ways for a face-on disk, these effects cause a decrease in T_{bb} (by a factor of 2.5/2) and an increase in r_{bb}. Corrections to remove Compton and GR effects from the data points are, hence, $\Delta \log T_{bb} \lesssim +0.1$ and $\Delta \log r_{bb} \lesssim -0.2$, which is indicated by the lower-

right-ward arrow in figure 4. (Since a model predicts lower $T_{\rm bb}$ by these effects, we need a higher $\dot{m}$ to reproduce the observed $T_{\rm bb}$.)

For disks with non-zero inclination angles around a Schwarzschild black hole, Doppler boosting enhances the radiation, yielding, at most, a factor of ~ 1.4 *increase* in $T_{\rm bb}$ compared with face-on disks, while the total flux remains roughly constant (Sun, Malkan 1989). We thus expect a slight *increase* in $T_{\rm bb}$ and a *decrease* in $r_{\rm bb}$ for a fixed $r_{\rm bb}^2 T_{\rm bb}^4$, compared with face-on disks. Required corrections are $\Delta \log T_{\rm bb} \lesssim -0.2$ and $\Delta \log r_{\rm bb} \lesssim +0.4$, which is indicated by the arrow pointed toward the upper-left in figure 4.

It is evident in figure 4 that all NLS1s have a relatively large $\dot{m}$. In other words, NLS1s shine at luminosities close to the Eddington limit (Hayashida 2000). Especially, PG 1404, H 0707, and IRAS 13224, all having a large $\dot{m}$ in figure 4, and enhanced soft components are known to exhibit a giant amplitude variability. In fact, Hayashida (2000) found that the mass estimated by the variability (Hayashida et al. 1998) significantly deviates from that estimated by equating $r_{\rm bb} = 0.5\, r_{\rm S}$ in those sources, suggesting anomalously large variability amplitudes compared with other NLS1s with a similar black-hole mass. This tendency indicates a correlation between $L/L_{\rm E}$ and the variability amplitudes (and soft X-ray excess over hard X-rays, see below).

Despite the ambiguities in the data points in figure 4, we may conclude that all (or, at least, most of) the NLS1s fall on the region with $\dot{m} > 10$, supporting our view that slim disks emit a substantial fraction of soft X-rays at $\sim L_{\rm E}$ in NLS1s. The observed steep slopes, $a_{\rm os}$ (see subsection 3.2), rather enhances our conclusion concerning a high $\dot{m}$, since it means more optical radiation, and thus a higher $\dot{m}$, than that expected solely from X-rays.

4. Variability of NLS1s

The strength of the soft excess is correlated with the variability amplitudes; objects with strong soft excesses show higher amplitude variability (Leighly 1999b). Hence, successful models for NLS1s should account for the presence of soft X-ray variability. Leighly (1999a) has summarized the ASCA observations of NLS1s, finding a systematically large excess variance in NLS1s. This fact can be, in principle, explained in terms of small black-hole masses; however, the origin of the giant-amplitude variations observed in some NLS1s, including IRAS 13224–3809 (Boller et al. 1997; see also Otani et al. 1996) and PHL 1092 (Brandt et al. 1999), seems to require an additional explanation (see subsection 3.5). The lack of optical variability in IRAS 13224−3809 poses a problem (Young et at. 1999), although both the soft and hard components (in the ASCA band) are known to vary nearly simultaneously in the same source (Otani et al. 1996). Relativistic boosting of otherwise modest variations may produce extreme variability of this source (Boller et al. 1997).

The light curves of NLS1s, especially those exhibiting extreme variations, have the following characteristics:
(1) The light curves seem to be composed of numerous flares (or shots).
(2) The flares do not have an identical time profile, but show a variety of flare amplitudes and durations.
(3) The temporal distribution of each flare is apparently random.

Interestingly, these features are the same as those found in GBHC during the low (hard) and very high states (see, e.g., van der Klis 1995). Fluctuations in the soft X-ray component (of a disk origin) are observed only in the very high state, while the low-state disk has no soft component. In this sense, NLS1s are more like GBHC during the very high state.

To reproduce theses characteristics of the light curves, Kawaguchi et al. (2000) proposed that a fractal magnetic-field structure spontaneously arises in an optically thin, advection-dominated flow and produces sporadic magnetic flare events, like solar flares, via magnetic reconnection. In fact, the dynamics of the magnetic fields in ADAFs is known to be well represented by a cellular-automaton model based on the notion of the self-organized criticality (Mineshige et al. 1994b; Kawaguchi et al. 1998). It is of great importance to note that both of the optically thick and thin ADAFs may share common time-dependent properties, since they are both dynamical systems in the sense that the radial accretion velocity, v_r, is comparable to the free-fall velocity and sound speed, as long as α is not small. We, here, argue that the same MHD model can be relevant to the slim disk, thus explaining the variability of NLS1s, as well.

If the fluctuations are of magnetic origin, large-amplitude fluctuations indicate relatively large field energy compared to the radiation energy. Suppose that gas cloud of a unit mass falls onto a black hole. Since radiative cooling is efficient in the standard-type disk, energy that is emitted away is comparable to the release of the gravitational energy, $E_{\rm rad} \sim E_{\rm grav} (\sim GM/r)$. As a result, the internal energy of the gas should be much lower than the gravitational energy, $E_{\rm gas} \ll E_{\rm grav}$. Since the magnetic field energy will be, at most, on the same order as the gas energy, $E_{\rm mag} \lesssim E_{\rm gas}$, we have $E_{\rm mag} \ll E_{\rm grav} \sim E_{\rm rad}$. If fluctuations occur due to a sporadic release of magnetic energy via magnetic reconnection, this inequality explains small fluctuations in the standard disk.

In the ADAF state, both optically thick and thin ones, radiative cooling is inefficient. Suppose again that a gas cloud of unit mass falls onto a black hole. A distinction exists in what carries energy to a hole; it is internal energy of gas for the case of the optically

thin ADAF, whereas it is trapped photons for the slim disks. In any case, the internal energy of gas or of trapped photons is of the order of the gravitational energy, which greatly exceeds the radiation energy which is emitted away, $(E_{\rm rad})_{\rm trapped} > (E_{\rm rad})_{\rm out}$. Since, again, $E_{\rm mag} \lesssim (E_{\rm rad})_{\rm trapped}$, a moderately large magnetic energy, compared with the energy radiated away, is expected, $E_{\rm mag} \gtrsim (E_{\rm rad})_{\rm out}$. The larger is $\dot{m}$, the greater becomes the ratio of $(E_{\rm rad})_{\rm trapped}/(E_{\rm rad})_{\rm out}$. Namely, large fluctuations in soft X-ray emission are inevitable at high $\dot{m}$, consistent with the observations of NLS1s.

In contrast, the standard-type disk (which may exist in BLS1s) is stable and, hence, is not variable. Fluctuations from BLS1s are thus due to a variation of the incident power-law radiation from the disk coronae, which are presumably filled with magnetic fields, and are thus variable for the same reason as that mentioned above. In terms of variability, therefore, the disk main body is passive in BLS1s, while it is active in NLS1s. To elucidate the theory distinguishing these two, however, realistic modeling of the disk-corona structure is needed as future work.

5. Outstanding Issues

5.1. *Radiation Transfer*

In a hot and dense layer with a very large Thomson depth (τ), there are several important effects to be considered in addition to Compton-scattering effects. First, the photon diffusion time ($\sim H\tau/c$) may exceed the accretion time.

$$\tau_{\rm dif} \simeq 4 \times 10^4 \Sigma_4 (H/r)(r/10\ r_{\rm S}) M_5\ {\rm s} \tag{10}$$

and

$$\tau_{\rm acc} \simeq 5 \times 10^2 (v_r/0.1\ v_{\rm ff})^{-1} (r/10\ r_{\rm S})^{3/2} M_5\ {\rm s}, \tag{11}$$

where $\Sigma_4 \equiv \Sigma/10^4$ g cm^{-2} and v_r is the accretion (radial) velocity. Then, the amount of photons which can be emitted to space is limited so that the disk luminosity becomes even lower, say below $L_{\rm E}$, even for large $\dot{m}$. Even though such effects as those arising due to a finite diffusion time are omitted in the present study, this treatment is reasonable if efficient convective mixing of gas and radiation occurs so that photons generated on the equatorial plane can reach the disk surface on dynamical timescales. Such effects should be examined in the future, however.

Second, thermalization timescales may exceed the accretion time for $\alpha \gtrsim 0.03$ (Beloborodov 1998). Then, the disk temperature becomes remarkably high, $\sim 10^8$ K, even for the parameters of AGN, producing much higher energy radiation. However, such high-energy emission spectra do not reconcile with the observed soft spectra of NLS1s with a soft excess of $kT \sim 100$ eV. Probably, again, convective mixing of gas and radiation promotes rapid thermalization between them. Or, alternatively, the viscosity parameter could be small, $\alpha < 0.03$, for which thermalization could occur within the accretion time.

Finally, the radiation field is more likely to be anisotropic; i.e., radiation mostly goes out in the vertical direction to the disk plane, whereas matter approaches to the black hole along the disk plane. This greatly reduces the flux to an observer viewed from a direction with large inclination angles. Sub-Eddington luminosity is expected even when the total, L, exceeds $L_{\rm E}$.

5.2. *Limit-Cycle Oscillations*

Since the standard and slim-disk branches form an **S**-shape in the thermal equilibrium curves (Abramowicz et al. 1988), there is a possibility of limit-cycle oscillations between the two branches (Honma et al. 1991; Szuszkiewicz, Miller 1998). Such oscillations, if they occur, will possibly explain any quasi-periodic outburst behavior, which may explain transient AGN phenomena in otherwise normal (inactive) galactic nuclei (see, e.g., Komossa, Bade 1999; Komossa, Greiner 1999), although repeated outbursts will produce permanent AGN-typical NLR emission lines, which are not observed in some sources. Alternatively, the **S**-shaped curve may produce soft-hard transitions; i.e., transitions from the slim disk to the optically thin ADAF (Takeuchi, Mineshige 1998). These possibilities should be elucidated in the future.

5.3. *Implications on Cosmological Evolution*

It is often argued that for a BH to increase its mass by a factor of $\sim e$ it takes $t_{\rm E} \equiv M/\dot{M}_{\rm E} \sim 10^8$ yr, since the maximum accretion rate onto a BH is regulated by the Eddington rate, $\dot{M}_{\rm E} \sim 10 L_{\rm E}/c^2$. Then, it takes quite a long time, $\sim 2 \times 10^9$ yr, to make a $10^9 M_\odot$ BH out of $\sim 10 M_\odot$ BH. A much shorter time is sufficient, however, if supercritical accretion is allowed. Indeed, supercritical accretion is unavoidable to account for the present quasar population (e.g., Kauffmann, Haehnelt 1999). It might be that there used to be numerous NLS1s in the past. The observational consequences need to be investigated.

6. Conclusions

To summarize, we have discussed various aspects of a slim disk in the context of NLS1s in comparison with the other disk models (see table 3). The following are the main conclusions:

1. The disk begins to exhibit the slim-disk properties when the luminosity moderately exceeds $L_{\rm E}$. Then, a substantial amount of radiation is expected to originate from inside the marginally stable last circular orbit at $3\ r_{\rm S}$. Therefore, a small $r_{\rm bb} < 3\ r_{\rm S}$ does not necessarily mean the presence of a Kerr hole.

Table 3. Basic disk models and their properties.

Disk models	Standard disk ($\tau > 1$)	ADAF ($\tau < 1$)	ADAF ($\tau > 1$)
Energy balance	$Q_{\rm vis} = Q_{\rm rad} \gg Q_{\rm adv}$	$Q_{\rm vis} = Q_{\rm adv} \gg Q_{\rm rad}$	$Q_{\rm vis} = Q_{\rm adv} \gg Q_{\rm rad}$
Disk height	$H \ll r$	$H \lesssim r$	$H \lesssim r$
Electron temperature	$\sim 10^6 M_5^{-\frac{1}{4}} (r/r_{\rm S})^{-\frac{3}{4}}$K	$\lesssim 10^{10}$K	$\sim 2 \times 10^6 M_5^{-\frac{1}{4}} (r/r_{\rm S})^{-\frac{1}{2}}$K
Ion temperature	$\sim 10^6 M_5^{-\frac{1}{4}} (r/r_{\rm S})^{-\frac{3}{4}}$K	$\sim 10^{12} (r/r_{\rm S})^{-1}$K	$\sim 2 \times 10^6 M_5^{-\frac{1}{4}} (r/r_{\rm S})^{-\frac{1}{2}}$K
Luminosity	$L \propto \dot{M}$	$L \propto (\dot{M})^2$	$L \propto \ln \dot{M}$
Spectrum	blackbody	power-law	blackbody
Final energy form	emitted radiation	internal energy of gas	trapped radiation
Magnetic energy	$E_{\rm mag} \ll E_{\rm grav} \sim E_{\rm rad}$	$E_{\rm mag} \sim E_{\rm grav} \gg E_{\rm rad}$	$E_{\rm mag} \sim E_{\rm grav} > E_{\rm rad}$
Fluctuation	small	large	large

2. If we fit the spectrum of the slim disk with the disk blackbody model, the derived size of the X-ray emitting region will be $r_{\rm in} \lesssim 3\, r_{\rm S}$ and the maximum temperature will be $kT_{\rm in} \sim 0.2\ M_5^{-1/4}$ keV. Further, p ($\equiv d \ln T_{\rm eff}/d \ln r$) decreases from 0.75 to ~ 0.5 as $\dot{M}$ increases.

3. All of the ASCA data of NLS1s fall on the region with supercritical accretion, $\dot{m} > 10$, supporting that the disks in NLS1s are likely to be slim disks.

4. The slim disk can also produce large fluctuations because the release of magnetic-field energy (which will produce fluctuations via magnetic flares) dominates over the energy release due to persistent emission.

We are grateful for A. Laor and an anonymous referee for useful comments. This work was supported in part by the Grants-in Aid of the Ministry of Education, Science, Sports and Culture (10640228, SM).

References

Abramowicz M.A., Czerny B., Losota J.P., Szuszkiewicz E. 1988, ApJ 332, 646
Beloborodov A.M. 1998, MNRAS 297, 739
Boller Th., Brandt W.N., Fabian A.C., Fink H.H. 1997, MNRAS 289, 393
Boller Th., Brandt W.N., Fink H. 1996, A&A 305, 53
Boroson T.A., Green R.F. 1992, ApJS 80, 109
Brandt N., Boller T. 1998, Astron. Nachr. 319, 163
Brandt W.N. 1999, in High Energy Processes in Accreting Black Holes, ed J. Poutanen, R. Svensson (ASP Conf. Ser. 161) p166
Brandt W.N., Boller T., Fabian A.C., Ruszkowski M. 1999, MNRAS 303, L53
Brandt W.N., Laor A., Wills B.J. 2000, ApJ 528, 637
Brandt W.N., Mathur S., Elvis M. 1997, MNRAS 285, L25
Czerny B., Elvis M. 1987, ApJ 321, 305
Edelson R., Vaughan S., Warwick R., Puchnarewicz E., George I. 1999, MNRAS 307, 91
Fukue J. 2000, PASJ submitted
Grupe D., Beuermann K., Mannheim K., Thomas H.-C. 1999, A&A 350, 805
Grupe D., Beuermann K., Thomas H.-C., Mannheim K., Fink H.H. 1998, A&A 330, 25
Halpern J.P., Oke J.B. 1987, ApJ 312, 91
Hayashida K. 2000, in Proc. COSPAR Meeting: Broad Band X-Ray Spectra of Cosmic Sources, ed K. Makishima, Adv. Space Res. 25, p489
Hayashida K. Miyamoto S., Kitamoto S., Negoro H., Inoue H. 1998, ApJ 500, 642
Honma F., Matsumoto R., Kato S. 1991, PASJ 43, 147
Kaspi S., Smith P.S., Maoz D., Netzer H., Jannuzi B.T. 1996, ApJ 471, L75
Kato S., Fukue J., Mineshige S. 1998, Black-Hole Accretion Disks (Kyoto University Press, Kyoto)
Kauffmann G., Haehnelt M. 1999, astro-ph/9906493
Kawaguchi T., Mineshige S., Machida M., Matsumoto R., Shibata K. 2000, PASJ 52, L1
Kawaguchi T., Mineshige S., Umemura M., Turner E.L. 1998, ApJ 504, 671
Komossa S., Bade N. 1999, A&A 343, 775
Komossa S., Greiner J. 1999, A&A 349, L45
Laor A. 1998, astro-ph/9810227
Laor A., Fiore F., Elvis M., Wilkes B.J., McDowell J.C. 1997, ApJ 477, 93
Leighly K.M. 1999a, ApJS 125, 297
Leighly K.M. 1999b, ApJS 125, 317
Leighly K.M., Mushotzky R.F., Yaqoob T., Kunieda H., Edelson R. 1996, ApJ 469, L147
Matsumoto R., Kato S., Fukue J., Okazaki A.T. 1984, PASJ 36, 71
Mineshige S., Hirano A., Kitamoto S., Yamada T.T., Fukue J. 1994a, ApJ 426, 308
Mineshige S., Kusunose M., Matsumoto R. 1995, ApJ 445, L43
Mineshige S., Takeuchi M., Nishimori H. 1994b, ApJ 435, L125
Narayan R., Yi I. 1995, ApJ 444, 231
Osterbrock D.E., Pogge R.W. 1985, ApJ 297, 166
Otani C., Kii T., Miya K. 1996 in Röntgenstrahlung from the Universe, ed H.U. Zimmermann, J.E. Trümper, H. Yorke, MPE Report 263, p491

Paczyński B., Wiita P.J. 1980, A&A 88, 23
Pounds K.A., Done C., Osborne J.P. 1996, MNRAS 277, L5
Ross R.R., Fabian A.C., Mineshige S. 1992, MNRAS 258, 189
Rybicki G.B., Lightman A.P. 1979, Radiative Processes in Astrophysics (John Wiley & Sons, New York) ch7
Shakura N.I., Sunyaev R.A. 1973, A&A 24, 337
Shimura T., Takahara F. 1995, ApJ 440, 610
Sun W.-H., Malkan M.A. 1989, ApJ 346, 68
Szuszkiewicz E., Malkan M.A., Abramowicz M.A. 1996, ApJ 458, 474
Szuszkiewicz E., Miller J.C. 1998, MNRAS 298, 888
Takeuchi M., Mineshige S. 1998, ApJ 505, L19
Tanaka Y. 1989, in Proc. 23 ESLAB Symp. on Two Topics in X-Ray Astronomy, ed J. Hunt, B. Battrick, ESA SP-296, p3
van der Klis M. 1995, in X-Ray Binaries, ed W.H.G. Lewin, J. van Paradijs, E.P.J. van den Heubel (Cambridge University Press, Cambridge) p252
Wang J.M., Szuszkiewicz E., Lu E.J., Zhou Y.-Y. 1999, ApJ 522, 839
Watarai K., Fukue J. 1999, PASJ 51, 725
Watarai K., Fukue J., Takeuchi M., Mineshige S. 2000, PASJ 52, 133
Wills B.J., Laor A., Brotherton M.S., Wills D., Wikes B.J., Ferland G.J., Shang Z. 1999, ApJ 515, L53
Young A.J., Crawford C.S., Fabian A.C., Brandt W.N., O'Brien P.T. 1999, MNRAS 304, L46